ELSEVIER

www.elsevier.nl/locate/carres

Carbohydrate Research 329 (2000) 141–155

CARBOHYDRATE RESEARCH

Solution conformation of various uridine diphosphoglucose salts as probed by NMR spectroscopy

Céline Monteiro, Sandrine Neyret, Jade Leforestier, Catherine Hervé du Penhoat *

Centre de Recherches sur les Macromolécules Végétales, CNRS (associated with University Joseph Fourier), BP 53, F-38041 Grenoble, France

Received 31 January 2000; accepted 25 May 2000

Abstract

The solution conformations of uridine diphosphoglucose (UDP-Glc) under a variety of conditions (solvent, ionic strength, various mono- and divalent cations) have been studied by NMR spectroscopy (^{1}H, ^{13}C, ^{31}P, and ^{25}Mg). In the case of divalent cations (Ca^{2+}, Mg^{2+}, Mn^{2+}) the phosphate oxygens are the preferred coordination sites and analysis of the ^{25}Mg linewidths of solutions with various $[Mg^{2+}]/[UDP\text{-}Glc]$ ratios, indicates that the 1:1 Mg^{2+}–UDP-Glc complex is the major species. From ^{13}C relaxation data and hydrodynamic theory, it has been demonstrated that under all conditions UDP-Glc adopts a fairly extended overall shape and that magnesium ions lead to a significant increase in the average length of the UDP-Glc molecule as compared to monovalent cations. Thus, one of the roles of the metal ion in enzymic reactions involving nucleotide sugars may be to preorganize the nucleotide sugar.

Keywords: Solution conformation; Uridine diphosphoglucose salts; NMR spectroscopy

1. Introduction

Glycosyl esters of nucleoside pyrophosphates, often referred to as sugar nucleotides, are major metabolites in the syntheses of glycans and glycoconjugates. They undergo many types of enzymatic reactions including transformation of the glycosyl group (epimerization, oxidation, reduction), splitting of the pyrophosphate linkage, and transfer of the glycosyl group to an acceptor [1]. The latter class of reactions, which are mediated by glycosyltransferases, proceed with remarkable selectivity as a unique sugar nucleotide (glycosyl donor) is stereoselectively transferred to a specific position of a given glycan or glycoconjugate (glycosyl acceptor). Due to the excellent yields of these processes, glycosyltransferases are now routinely used in the laboratory for the syntheses of complex carbohydrates [2,3]. In vivo these enzymes operate in the presence of a pool of sugar nucleotides and glycosyl acceptors. The high specificity of the reactions suggests that the recognition steps in the formation of both the nucleotide sugar–glycosyltransferase and glycosyl acceptor–glycosyltransferase complexes are of paramount importance.

In the case of uridine diphosphoglucose (UDP-Glc) (Fig. 1), which was first isolated by Leloir and coworkers [4,5], the effects of chemical modification of the various functional groups on the activities of different enzymes have been extensively studied. Ko-

* Corresponding author. Tel.: +33-476-037603; fax: +33-476-547203.

E-mail address: penhoat@cermav.cnrs.fr (C. Hervé du Penhoat).

0008-6215/00/$ - see front matter
PII: S0008-6215(00)00166-X

chetkov and coworkers [6] distinguished three classes of binding sites: (i) universally essential sites including the hydroxyl group at C-3″ and the acylamido group (CONHCO) of the uracil base, (ii) universally non-essential sites including the double bond of the heterocyclic base and the hydroxyl groups at C-2′ and C-2″, and (iii) specific sites essential for some enzymes and non-essential for others such as the hydroxyl groups at C-4″ and C-6″. They postulated the existence of a notable fraction of folded conformations stabilized by three intramolecular hydrogen bonds (O-2···H–O-2′, 3-N–H···O-3″, and O-4···H–O-2″) to explain their results. The existence of folded conformations was also advocated to explain optical rotation data for various sugar nucleotides including UDP-Glc. The change in optical rotation in going from an aqueous solution of UDP-Glc to an 8 M urea solution of UDP-Glc was interpreted as the reversible dissociation of an ordered to a random conformation [7]. However, subsequent NMR studies of UDP-Glc in aqueous solution indicated typical geometries for the various segments ($^4C_1$ form for glucose, a 1:1 mixture of C-2′-endo–C-3′-endo ribose conformers, and an anti orientation of the base) [8,9]. An extended overall shape was proposed from a ^{13}C NMR study using the lanthanide induced-shift technique [10]. In this latter work, the lanthanide ions were localized above the central oxygen of the pyrophosphate group.

The molecular conformation in crystalline disodium uridine diphosphoglucose contains similar features to those of the solution state for the sugar and base moieties ($^4C_1$ form for glucose; C-2′-endo puckering for ribose; trans, $^+$gauche and trans (anti) orientations of the β, γ, and χ torsion angles; the staggered form of the pyrophosphate group) [11]. However, the interactions between the sodium ions and UDP-Glc are very different and two coordination sites are observed. The first site includes O-2″ and a P_β oxygen of one molecule, the two base oxygens of a second molecule, and two coordinating waters. The second site contains four glucosyl oxygens (O-3″, O-4″, O-5″, and O-6″), O-2 of a second molecule and one water ligand.

Divalent metal cations such as Ca^{2+}, Mg^{2+} or Mn^{2+} are necessary for the catalytic activity of many of the enzymes which metabolize nucleotide sugars. Three crystal structures of glycosyltransferases (a β-glucosyl transferase [12], bovine β-(1→4)galactosyltransferase [13], and a putative glycosyltransferase [14]) have been reported to date and in the latter nucleotide sugar–enzyme complex Mn^{2+} was located near the phosphorous oxygen (P_β) of the nucleotide sugar. Certain metal ions (Ca^{2+}, Mg^{2+}, Fe^{3+}, Zn^{2+}, etc.) are known to strongly influence both secondary and tertiary nucleic acid structure [15,16] and it appeared conceivable that the role of the metal ion might be to preorganize the nucleotide sugar. Modeling of nucleotide sugar–metal interactions would be expected to afford a basis for understanding the role of the metal ion in nucleotide sugar–metal complexes. The pyrophosphate group has been studied with ab initio approaches [17–20] and force field parameters for both the CHARMM [17] and AMBER [19] molecular mechanics programs have been proposed. However, very little experimental data is available for validating the-

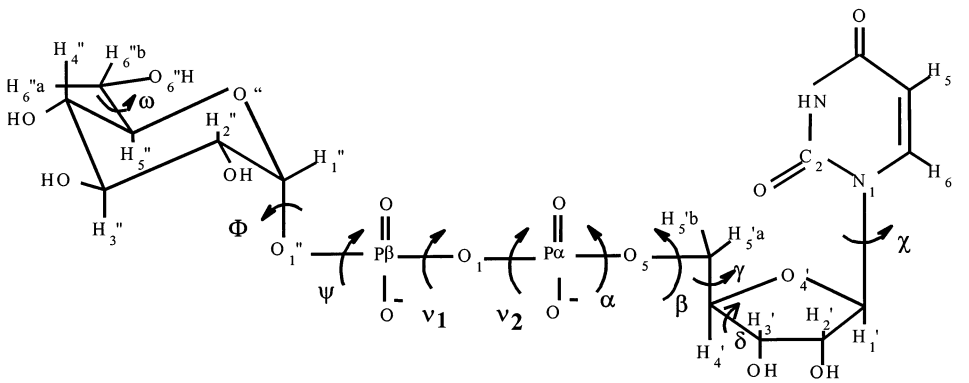

Fig. 1. Schematic drawing of UDP-Glc with atomic numbering and labels for the torsion angles of interest.

oretical models of these metabolites interacting with metal ions.

In the following study, a systematic investigation of the effect of various cations and solvant mixtures on the solution conformation of UDP-Glc was undertaken by NMR spectroscopy. The strategy adopted included: (1) determination of the localized conformational preferences through coupling constant data, and ^{1}H, ^{13}C and ^{31}P chemical shifts, (2) estimation of global molecular shapes of UDP-Glc through fitting of multi-field dipole–dipole carbon relaxation data with spectral densities suitable for a flexible molecule undergoing anisotropic overall tumbling [21–23] and conversion of the resulting correlation times into molecular dimensions on the basis of hydrodynamic theory, and (3) evaluation of the metal binding site either through diamagnetic shifts (alkaline earth cations), ^{25}Mg NMR or analysis of relaxation data in the presence of paramagnetic species (Mn^{2+}).

2. Material and methods

Nomenclature.—The atomic numbering and the usual torsion angle labels for UDP-Glc [16] have been indicated in Fig. 1. In keeping with the nomenclature used in the case of nucleoside diphosphates and triphosphates, the phosphorous atoms closest to the ribosyl and glucosyl moieties will be referred to as P_α and P_β, respectively. Three different arrangements have been described for the pyrophosphate group, cis-planar eclipsed, staggered and all-trans eclipsed (Fig. 2(a)). By analogy with the convention adopted for nucleoside pyrophosphates [16], metal chelates of UDP-Glc will be referred to as Δ-cis, Δ-trans, Λ-cis and Λ-trans (Fig. 2(b)).

The three preferred orientations of the glucosyl ω angle are referred to as gauche–gauche, GG ($-60°$), gauche–trans, GT ($+60°$) and trans–gauche, TG ($+180°$) [24]. The sign of the torsion angles are in agreement with the IUPAC–IUB conventions [25].

Sample preparation.—Uridine 5′-diphosphoglucose disodium salt (20 mg) was dissolved in 1 mL of a 10 mM aqueous solution of phosphate buffer containing 0.1% of EDTA and 1% of TSP (internal reference for the ^{1}H and ^{13}C spectra). This mixture was lyophilized three times against D_2O (99.8%, SDS) and then dissolved in 0.5 mL of D_2O (99.96%, SDS) and sealed in an NMR tube under argon after vacuum removal of dissolved oxygen. EDTA was omitted in the case of the divalent cations ($CaCl_2{\cdot}2H_2O$, $MgCl_2{\cdot}6H_2O$, $MnCl_2{\cdot}4H_2O$, Fluka).

NMR spectroscopy.—^{1}H and ^{13}C 1D spectra were acquired on various spectrometers (Bruker AC 300, Varian Unity 400, Bruker AM 400, and Varian Unityplus 500) at 25 °C. The digital resolution of the 1D proton and carbon spectra were ≤ 0.5 and 1 Hz/pt, respectively. ^{31}P NMR spectra were recorded at 25 °C with digital resolution of 0.2 Hz/pt (Bruker AC200, QNP probe; Varian Unity 400, double-resonance H/C probe equipped with a ^{31}P accessory). The lock signal did not drift during the entire session and therefore the series of spectra were referenced to the phosphate buffer offset frequency in the first spectrum (standard conditions — 33 mM UDP-Glc, 10 mM buffer, Na^+ and K^+ counterions). Two series of ^{25}Mg spectra were recorded at 24.5 MHz (Bruker AM400) with a multi-nuclear wide-band probe: one series in which the [Mg^{2+}]/[UDP-Glc] ratio was varied systematically (0.1–80) and another with a fixed [Mg^{2+}]/[UDP-Glc] ratio of 2 in which the temperature was increased in steps from 25 to 80 °C. T_1 measurements were conducted with the classical inversion-recovery sequence and 8–10 τ values ranging from 5 ms to 1.5 s with the exception of the runs conducted in the presence of Mn^{2+} where the τ values were shorter (5 ms to 1.2 s). In all cases at least two sets of data (generally four sets) were recorded to evaluate the experimental precision. Steady-state nuclear Overhauser effects were measured with irradiation times and pulse intervals greater than 5 times the longest proton T_1. A total of 512 transients were recorded with weak irradiation either at the frequency of interest or outside the spectral range and these FIDs were Fourier transformed with an exponential line broadening factor of 1 Hz in order to reduce noise.

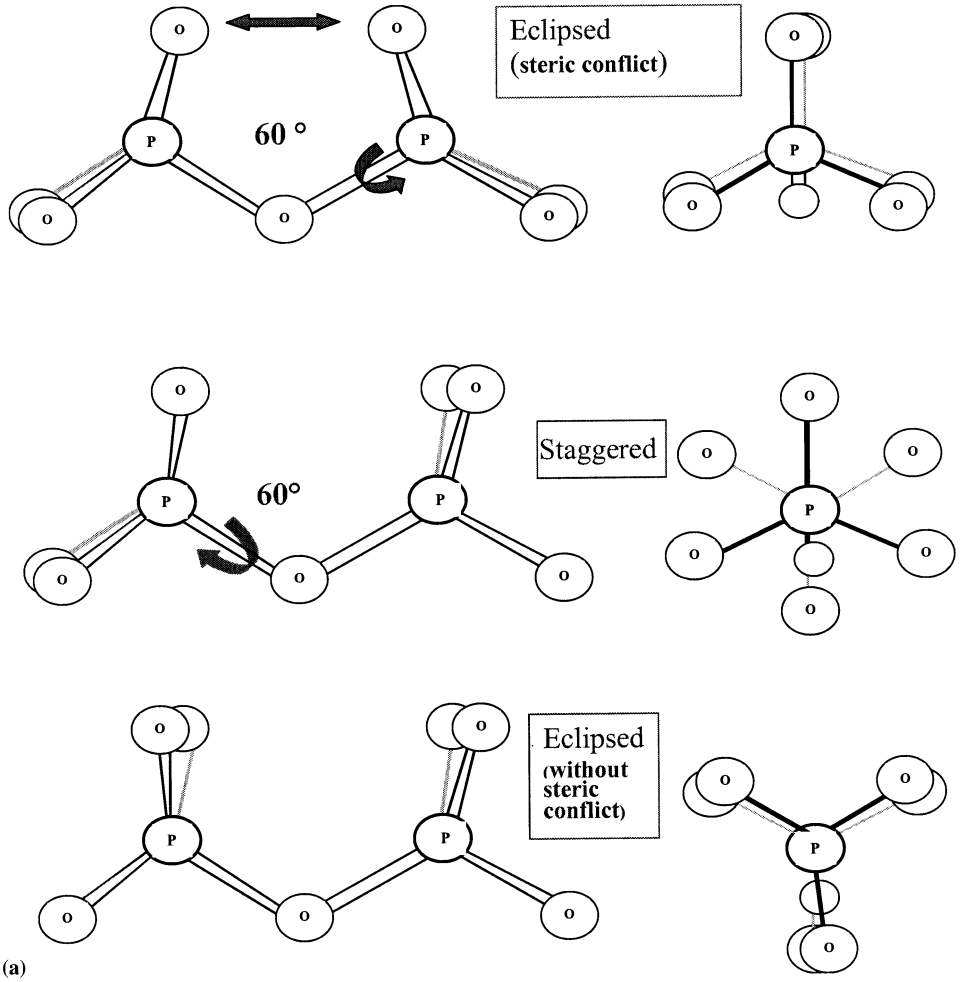

Fig. 2. (a) Eclipsed and staggered orientations of the pyrophosphate group. (b) Spatial arrangements of pyrophosphate chelates.

2D experiments were recorded on the aforementioned Varian spectrometers which were equipped with double-resonance H/C gradient probes. Quadrature detection was achieved in the non-acquisition dimensions by the TPPI [26] and the hypercomplex method [27] for the homonuclear and HMQC experiments, respectively. Phase-sensitive COSYDQF (1 Hz/pt) [28] and TOCSY spectra (1 Hz/pt; a MLEV-17 spinlock sequence corresponding to a 60-ms mixing time followed by a 2.5-ms trim pulse) [29] were acquired to assign the proton spectrum. Quantitative phase-sensitive NOESY spectra were recorded with mixing times 0 and 1 second and recycle times of 5.24 s. Phase-shifted squared sinebell apodization functions were applied in both dimensions and the first points were scaled. Data were zero-filled to 4096 and 2048 points in $F2$ and $F1$, respectively. A polynomial baseline correction was applied in $F2$ after Fourier transformation. Carbon assignments were obtained from the HMQC experiment (1 Hz/pt) [30].

NMR computational methods.—Theoretical carbon T_1 data were established at 75.13, 100.6 and 125 MHz with a flexible residue approach and typical values of the carbon–proton interatomic distance ($1.09 \leq r_{C-H} \leq 1.11$ Å) [31]. Internal motion was taken into account by using the full model-free spectral densities [23] appropriate for axially symmetric anisotropic overall motion [21,22] implemented in inhouse software.

$$\frac{1}{T_1} = K\{J_0(\omega_H - \omega_C) + 3J_1(\omega_C) + 6J_2(\omega_H + \omega_C)\}$$

$$J(\omega) = \frac{2}{5}\left\{S^2_{C-H}J_{an}(\omega) + \frac{(1 - S^2_{C-H})\tau}{1 + (\omega\tau)^2}\right\}$$

$$J_{an}(\omega) = \left\{0.25(3\cos^2\theta - 1)^2 \frac{\tau_a}{1 + (\omega\tau_a)^2}\right\} + \left\{(3\sin^2\theta\cos^2\theta)\frac{\tau_b}{1 + (\omega\tau_b)^2}\right\} + \left\{(0.75\sin^4\theta)\frac{\tau_c}{1 + (\omega\tau_c)^2}\right\}$$

$$\tau_a = \tau_\perp$$

$$1/\tau_b = 5/(6\tau_\perp) + 1/(6\tau_{//})$$

$$1/\tau_c = 1/(3\tau_\perp) + 2/(3\tau_{//})$$

where $K = \gamma^2_H\gamma^2_C/10r^6_{C-H}$, θ is the angle between the C–H vector and the major axis of the hypothetical cylinder encasing the UDP-Glc molecule, $\tau_\perp$ and $\tau_{//}$ are the rotational correlation times about the short and long axes of the cylinder, and τ is related to the effective correlation time, τ_e, of internal motion ($1/\tau = 1/\tau_e + 1/\tau_0$ where τ_0 is the molecular tumbling time). In this formalism the amplitude (S^2_{C-H}, angular order parameter) and the effective correlation time (τ_e) of the internal dynamics must be specified along with the molecular tumbling times ($\tau_\perp$ and $\tau_{//}$, axially symmetric anisotropic overall motion). Dynamic parameters were varied to optimize the fit between theoretical and experimental T_1 data ($0.5 < S^2_{C-H} < 0.9$; $50 < \tau_e < 200$ ps; τ_c, $\tau_\perp$ and $\tau_{//} \pm 50\%$ with respect to the values established from hydrodynamic theory, vide infra). The angles between the various carbon–proton vectors and the axis of the cylinder were estimated with inhouse software (FORTRAN) from the Cartesian coordinates of the crystal structure of disodium uridine diphosphoglucose dihydrate after reorientating the molecule about the axis of the principal inertial tensor with CHARMM-22 [32].

Proton diamagnetic cation induced shifts can be obtained from Buckingham's theory [33]:

$$\Delta\delta = k4.8(\cos\theta)/r^2$$

where r is the length (Å) of the vector from the charge to the middle of the C–H bond, θ is the angle between that vector and the C–H bond, and k is a proportionality constant, obtained empirically. This approach has been extended to include treatment of diamagnetic shifts for carbon by Batchelor [34].

In the case of certain paramagnetic relaxation reagents such as Mn^{2+}, a complex is formed between the paramagnetic species and the molecule of interest. Due to the long electron-spin relaxation rates ($T_{1e,2e} \sim 10^{-8}$ s in the case of Mn^{2+}) nuclear longitudinal relaxation rates of nearby nuclei are strongly enhanced while chemical shifts are not noticeably affected. An r^{-6} dependence on the nucleus–electron distance is observed in the equation describing the contribution to the

nuclear longitudinal relaxation rate from the component spin on the paramagnetic species [35,36].

Finally, expressions for the rotational diffusion coefficients, $D_r^{\perp}$ and $D_r^{//}$ have been reported for models of short cylinders [37,38] with anisotropic ratios, $p \geq 2$ ($p = L/d$, where L and d are the length and the diameter of the cylinder, respectively):

$$\pi\eta_0 L^3 D_r^{\perp}/3kT = \ln(p) + \delta_{\perp}$$

$$A_0\pi\eta_0 L^3 D_r^{//}/kT = p^2/(1 + \delta_{//})$$

where $A_0 = 3.84$, $\delta_{\perp} = -0.662 + (0.917/p) - (0.050/p^2)$, and $\delta_{//} = (0.677/p) - (0.183/p^2)$.

Molecular models.—A molecular model was constructed from the Cartesian coordinates of the crystal structure of disodium uridine diphosphoglucose [11] with the QUANTA-97 commercial package (MSI). The C–H distances were then arbitrarily set to 1.10 Å with the QUANTA-97 software to counter-balance the systematic errors associated with the proton positions in X-ray crystal structures. After setting the NMR-defined torsion angles to their experimental values (either C-2′-endo or C-3′-endo ribose puckering; Φ, β, γ and χ — vide infra) various internuclear distances were measured for two structures with the pyrophosphate group in either the trans staggered or the trans eclipsed conformation, respectively, while systematically exploring the torsion angles between the pyrophosphate group and the sugar moieties (Ψ and α) in 60° steps.

3. Results and discussion

Conformational analysis based on NMR coupling constant and NOE data.—The ^{1}H NMR assignments of UDP-Glc at pH 8 in D_2O have been reported previously [8] and the data given in Table 1 for solutions of UDP-Glc in various solvents (D_2O, DMSO-d_6, MeOH-d_4) and in the presence of alkali and alkali-earth cations (Na^+ and K^+, Mg^{2+}, Ca^{2+}) are analogous. The major conformational features established from vicinal coupling constants with Karplus-type relationships and from NOE data as discussed in earlier work [8] are as follows: the $^4C_1$ form for the pyranosyl ring, a predominant GG orientation of the glucosyl pendant group in aqueous solution with fairly equal populations of GG and GT rotamers in the organic solvents (DMSO-d_6, MeOH-d_4) [39,40], fairly equal C-2′-endo and C-3′-endo puckering populations for the ribosyl ring, strong preferences for the trans and g^+ rotamers for the β (76%) and γ (83%) torsion angles [41,42], typical anti orientations about the χ torsion angle ($-180 \leq \chi \leq -138°$ for C-3′-endo; $-144 \leq \chi \leq -115°$ for C-2′-endo) [16], and finally, a 90° orientation about the Φ [43]. This latter value also falls within the range of privileged orientations ($60° \leq \Phi \leq 135$) reported for the Φ angle of UDP-Glc with theoretical methods [19].

To complete the classical analysis based on coupling constant and NOE data, steady-state NOE difference spectra were recorded with low-power saturation of the H-5′a, H-5′b, and H-1″ signals (also H-4′, spectrum not given) for both the standard sample (monovalent cations) and the sample containing an equivalent of $MgCl_2$. The former series of difference spectra have been given in Fig. 3(a–c) and these experimental data allow an estimation of the time-averaged distance separating the sugar moieties. In the first two spectra (Fig. 3(a and b), the H-5′a, and H-5′b signals are saturated, respectively), very weak interactions between both of the ribosyl methylene protons and H-1″ are detected indicating an interatomic distance roughly between 4.5 and 5 Å. Close inspection of the former spectrum also reveals an intraresidue NOE between H-5′a and H-1′ whereas such an effect is not observed for H-5′b. The interatomic distances between H-5′proR and H-5′proS and the ribose anomeric protons were estimated from molecular models of UDP-Glc with the aforementioned NMR-defined conformational features (trans and g^+ rotamer orientations of the β and γ torsion angles) and the ribose sugar in either the C-2′-endo or C-3′-endo conformation. In both cases the H-5′proS–H-1′ distance ($\sim$4.6–4.7 Å) was shorter than the H-5′proR–H-1′ distance (4.9–5.2 Å) and accordingly the H-5′a signal has been tentatively assigned to H-5′proS.

Table 1
500 MHz ^{1}H [a] and 81 MHz ^{31}P [b] NMR chemical shift and coupling constant data for 33 mM buffered [c] solutions of UDP-Glc recorded under various conditions (solvent and counterion [d]) at 298 K

	Standard conditions: D_2O, 0.3 K^+, 2.7 Na^+	D_2O, 1 Mg^{2+}	D_2O, 1 Ca^{2+}	D_2O, 3 K^+, 9 Na^+	8 M urea in D_2O, 0.3 K^+, 2.7 Na^+	DMSO–D_2O 9/1 v/v, 0.3 K^+, 2.7 Na^+	MeOD–D_2O 4/1, 0.3 K^+, 2.7 Na^+
H-1″	5.68, dd	5.63, dd	5.63, dd	5.67, dd	5.70, dd	5.4, dd	4.18, dd
$J_{H\text{-}1''\text{–}P\beta}$	7.3	7.1	7.3	6.9	7.3	7.7	7.7
$J_{H\text{-}1''\text{–}H\text{-}2''}$	3.5	3.5	3.7	3.5	3.7	4.0	3.6
H-2″	3.60, ddd	3.57, ddd	3.57, ddd	3.60, ddd	3.62, ddd	3.13, ddd	1.92, ddd
$J_{H\text{-}2''\text{–}P\beta}$	3.3	3.1	3.3	3.5	2.9	2.6	2.9
$J_{H\text{-}2''\text{–}H\text{-}3''}$	9.8	9.9	9.5	9.7	9.9	9.9	9.5
H-3″	3.84, dd	3.79, dd	3.81, dd	3.85, dd	3.85, c	3.45, dd	2.35, dd
$J_{H\text{-}3''\text{–}H\text{-}4''}$	9.7	9.7	9.5	10.1	9.5	9.1	10.9
H-4″	3.54, t	3.49, t	3.49, t	3.53, t	3.56, t	3.03, t	1.83, c
$J_{H\text{-}4''\text{–}H\text{-}5''}$	9.7	9.7	9.5	10.1	9.5	9.1	10.9
H-5″	4.00, c	3.91, c	3.94, c	3.99, c	4, c	3.48, c	2.44, c
$J_{H\text{-}5''\text{–}H\text{-}6''a}$	2	1.1		2.4	2.2		1.8
$J_{H\text{-}5''\text{–}H\text{-}6''b}$	4.4			4.9	4.4	6.6	5.8
H-6″a	3.96, d	3.83, c	3.89, dd	3.93, dd	3.93, c	3.76, dd	2.36, dd
$J_{H\text{-}6a''\text{–}H\text{-}6b''}$	12.4	12.8	10.2	12.8	11.7	12.1	11
H-6″b	3.88, c	3.80, dd	3.81, dd	3.85, d	3.92, d	3.45, c	2.2, d
H-1′	6.07, d	6.20, d	6.00, c	6.06, c	6.07, c	5.77, c	4.49, t
$J_{H\text{-}1'\text{–}H\text{-}2'}$				3.5		2.9	5.1
H-2′	4.45, c	4.30, c	4.40, c	4.46, c	4.45, c	4.07, dd	2.81, t
$J_{H\text{-}2'\text{–}H\text{-}3'}$						5.5	
H-3′	4.45, c	4.39, c	4.40, c	4.46, c	4.45, c	4.07, dd	2.89, c
$J_{H\text{-}3'\text{–}H\text{-}4'}$		3.3				5.1	
H-4′	4.36, c	4.31, c	4.31, c	4.36, c	4.37, c	3.64, c	2.69, c
$J_{H\text{-}4'\text{–}H\text{-}5'a}$	2.6						
H-5′a	4.31, c	4.28, c	4.31, c	4.26, c	4.32, c	3.63, c	2.76, c
$J_{H\text{-}5'a\text{–}P\alpha}$	4.5	2.4					4.4
$J_{H\text{-}5'a\text{–}H\text{-}5'b}$	11.8						
H-5′b	4.25, c	4.22, c	4.26, c	4.24, c	4.26, c	3.63, c	2.76, c
$J_{H\text{-}5'b\text{–}P\alpha}$	5.5			5.4	5.5	4.4	4
$J_{H\text{-}5'b\text{–}H\text{-}4'}$	3			2.9	2.9		2.7
H-5	6.05, c	5.99, d	6.01, d	6.03, c	6.05, c	5.74, d	4.43, d
H-6	8.02, d	7.96, d	7.98, d	8.01, d	8.01, d	7.85, d	6.54, d
$J_{H\text{-}6\text{–}H\text{-}5}$	8.1	8.0	8.0	8.0	8.0	8.0	8.0
P_α	−12.14	−12.33	−12.20				
P_β	−13.78	−14.01	−13.87				

[a] Referenced to the residual solvent proton signal: HOD, 4.8 ppm; methanol-d_4, 3.4 ppm; DMSO-d_6, 2.5 ppm.
[b] Standard sample, PO_4^{3-} 0.00 ppm (reference offset for divalent cations).
[c] 10 mM phosphate buffer.
[d] In equivalents with respect to UDP-Glc.

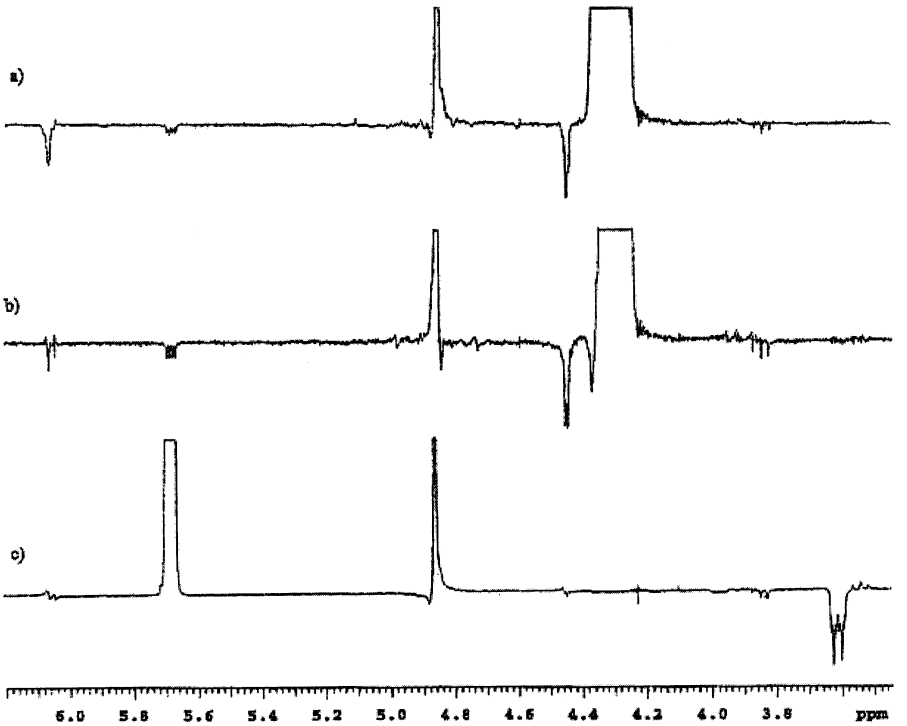

Fig. 3. 400 MHz steady-state NOE difference spectra of a 33 mM sample of UDP-Glc under standard conditions (10 mM phosphate buffer in D_2O, 0.3 equiv of K^+, 2.7 equiv of Na^+) at 298 K acquired with irradiation of (a) H-5′proS, (b) H-5′proR and (c) H-1″, respectively.

Overall molecular dimensions based on ^{13}C relaxation measurements and hydrodynamic theory.—In the case of fairly small molecules with overall molecular rotational reorientation times in the range 0.1–0.6 ns, a satisfactory description of molecular dynamics can be obtained by fitting multi-field methine carbon longitudinal relaxation data [44]. The main relaxation pathway is the dipole–dipole mechanism and the theoretical T_1 values are readily expressed in terms of spectral densities appropriate for a flexible molecule undergoing either isotropic (spherical shape proposed for a folded molecule [6,7,20]) [23] or axially-symmetric anisotropic molecular tumbling (quasi cylindrical shape postulated for an extended molecule [8,9]) [21,22]. From the resulting descriptors of rotational diffusion ($D_r^{\perp} = (6\tau_{\perp})^{-1}$, $D_r^{//} = (6\tau_{//})^{-1}$) it is then possible to deduce the time-averaged molecular shape from hydrodynamic theory [37,38]. In this context fitting of methine relaxation data offers two main advantages: (1) relaxation is mainly due to the dipole–dipole interaction with the directly attached proton and the corresponding internuclear distance can be considered to be fixed (1.11 Å [31]), and (2) due to the low abundance of the ^{13}C nuclei one is dealing with an isolated spin system and both higher spin-order and spin diffusion can be neglected.

The experimental multi-field carbon longitudinal relaxation times for the standard sample (Na^+/K^+) and for the one containing an equivalent of Mg^{2+} have been collected in Table 2. Methine T_1 parameters were significantly lower for samples containing Mg^{2+} ions (tubes prepared with either 1 or 2 equivalents of Mg^{2+}) when compared to those of solutions with only monovalent cations (either 10 or 100 mM buffer samples) and these variations in the relaxation data were highly reproducible. Perusal of the data in Table 2 reveals a considerable spread (20–30%) in T_1 parameters for both types of samples (Na^+/K^+ and Mg^{2+}) at all magnetic field strengths incompatible with isotropic overall tumbling. Accordingly, theoretical data were established for axially-symmetric anisotropic tumbling at all three magnetic field strengths after establishing the angles made by the C–H vectors with respect to the principal axis of inertia as

described in Section 2. These theoretical data were fitted to the experimental ones by exploring physically realistic ranges of the dynamic parameters (S^2, τ, $\tau_\perp$, $\tau_{//}$). Angular order parameters reported for both disaccharides [45] and triribonucleotides [46] lie between 0.5 and 0.8 while correlation times for internal motion are within the 30–200 ps range. Motional models were considered to be satisfactory when the summed squares of the deviations between the experimental and calculated T_1 values (referred to as R_f) were within the range of the summed squares of the experimental deviations (standard sample, $R_f^{expt} = 0.010$; Mg^{2+}, $R_f^{expt} = 0.007$).

In the case of the sample containing an equivalent of Mg^{2+} good agreement ($R_f = 0.01$) was obtained for the following values of the dynamic parameters: 50 ps, 0.24 ns, 0.12 ns, and 0.7 for τ, $\tau_\perp$, $\tau_{//}$, and S^2, respectively. Slightly shorter correlation times were required to reproduce ($R_f = 0.013$) the experimental data for the standard sample (50 ps, 0.18 ns, 90 ps, and 0.6 for τ, $\tau_\perp$, $\tau_{//}$, and S^2, respectively) suggesting a smaller time-averaged molecular volume. The molecular dimensions were then deduced from the corresponding rotational diffusion coefficients according to the equations proposed for short cylindrical objects by de la Torre and coworkers [37,38]. A more extended cylinder (length 17.2 Å and radius 4.3 Å) is found in the case of the sample containing an equivalent of Mg^{2+} than for the standard sample (length 15.2 Å and radius 4.0 Å) (Fig. 4). It is to be noted that reasonable fits to the experimental data set were observed for S^2 values between 0.6 and 0.9 whereas lower S^2 values (< 0.6, corresponding to more flexible models) gave both a poor fit and much too large overall molecular dimensions (vide infra).

The more significant sources of error in the estimation of the time-averaged molecular dimensions based on T_1 data and hydrodynamic theory were expected to be: (1) neglect of cross-correlation (DD/CSA) in the treatment of the NMR relaxation data [47], (2) neglect of a microviscosity correction factor, f, to account for departure from ideal conditions where the ratio of the solvent radius to that of the dissolved molecule is very small (≤ 0.01) and the solvent can be treated as a continuous medium characterized by a bulk viscosity [48], and (3) the choice of the carbon–proton inter-

Table 2
Multi-field carbon longitudinal relaxation times (ms), chemical shifts (ppm) and heteronuclear ^{13}C–^{31}P coupling constants (Hz) for 33 mM buffered solutions of UDP-Glc recorded at 298 K in the presence of 2.7 and 0.3 equiv of Na^+ and K^+, and 1 equiv of Mg^{2+}, respectively [a]

	Mg^{2+}				Standard conditions: 2.7 and 0.3 equiv of Na^+ and K^+			
	75 MHz	100.6 MHz	125 MHz	δ (ppm)	75 MHz	100.6 MHz	125 MHz	δ (ppm)
C-1″	446 ± 18	457 ± 19	549 ± 13	96.38	495 ± 39	511 ± 16	538 ± 38	96.34
$^2J_{C1''-1}$				7.3				6.1
C-2″	382 ± 23	486 ± 38	473 ± 16	72.25	469 ± 29	484 ± 9	573 ± 14	72.36
$^3J_{C2''-P1}$				8.5				8.5
C-3″	458 ± 4	458 ± 13	426 ± 37	73.59	512 ± 17	495 ± 9	463 ± 43	73.6
C-4″	409 ± 15	446 ± 14	465 ± 18	69.88	473 ± 25	473 ± 7	517 ± 13	69.94
C-5″	430 ± 12	441 ± 9	461 ± 11	73.55	441 ± 14	483 ± 3	506 ± 39	73.57
C-6″	255 ± 13	268 ± 4	282 ± 8	61.03	286 ± 11	292 ± 3	327 ± 14	61.07
C-1′	419 ± 11	434 ± 27	433 ± 44	89.28	406 ± 14	433 ± 3	474 ± 4	89.15
C-2′	512 ± 14	503 ± 15	478 ± 37	74.5	541 ± 25	535 ± 4	560 ± 27	74.54
C-3′	433 ± 38	474 ± 16	542 ± 33	70.34	490 ± 10	502 ± 9	533 ± 6	70.4
C-4′	408 ± 14	435 ± 14	469 ± 34	83.86	462 ± 14	442 ± 10	460 ± 33	83.99
$^3J_{C4'-P2}$				8.5				8.5
C-5′	221 ± 12	232 ± 10	240 ± 28	65.74	247 ± 8	242 ± 2	279 ± 19	65.7
$^2J_{C-5'-P-2}$				6.1				4.9
C-5	454 ± 15	454 ± 17	449 ± 15	103.4	441 ± 22	437 ± 6	462 ± 35	103.44
C-6	365 ± 21	388 ± 14	396 ± 33	142.38	393 ± 25	398 ± 6	410 ± 11	142.38

[a] The C-6 signal was set to 142.38 ppm in all spectra.

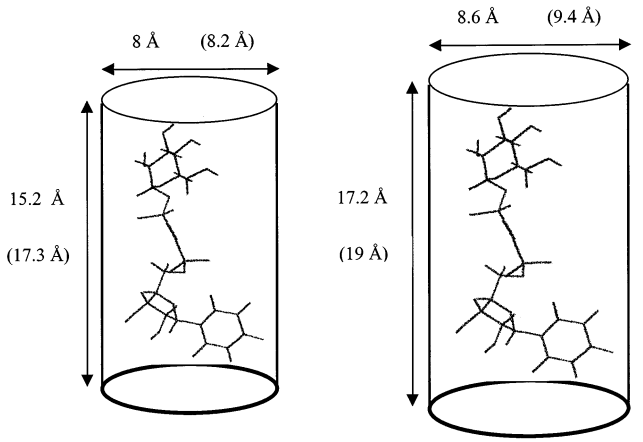

Fig. 4. Molecular dimensions (length and radius of the hypothetical cylinder encasing UDP-Glc) obtained from hydrodynamic theory and the motional models which were calculated from multi-field ^{13}C longitudinal relaxation data (r_{C-H} 1.11 Å): (left) of the standard sample and (right) of the sample containing 1 equiv of $MgCl_2$. The values in parentheses correspond to the motional models that were adjusted to take into account cross-correlation (CSA-DD mechanism).

atomic distance for the methine carbons [31]. In the case of the standard sample of UDP-Glc, the relevance of DD/CSA cross-correlation has been demonstrated through measurement of apparent T_1 values for the various lines of the multiplets for the methine and methylene signals in a proton-coupled carbon T_1 experiment (Table 3). It has been shown that the difference in high field relaxation behavior of the outer lines in the methylene multiplet results from dipolar-CSA cross-correlation [49]. To estimate the errors in overall molecular shape due to neglect of this latter relaxation pathway the experimental data in Table 2 were arbitrarily reduced by 15% (such a reduction has been measured for a pentasaccharide [50] with a pulse sequence which suppresses DD/CSA cross-correlation [51,52]) and theoretical data were fitted to this new set of T_1 data. In the case of the sample containing an equivalent of Mg^{2+}, good agreement ($R_f = 0.0075$) was obtained for the following values of the dynamic parameters: 50 ps, 0.32 ns, 0.16 ns, and 0.6 for τ, $\tau_\perp$, $\tau_{//}$, and S^2, respectively. Fitting of this 'corrected' dynamic model to the expressions for rotational diffusion revealed an increase in the time-averaged molecular volume of UDP-Glc (length 19.0 Å and radius 4.7 Å). The same tendancy was observed when the T_1 data for the standard sample (Na^+/K^+) were arbitrarily reduced in a similar manner (50 ps, 0.24 ns, 0.11 ns, and 0.6 for τ, $\tau_\perp$, $\tau_{//}$, and S^2, respectively, leading to a length of 17.3 Å and a radius of 4.1 Å) and the results of these calculations have been given in Fig. 4 (numbers in parentheses). Simulations also revealed that neglect of a microviscosity correction factor also leads to an under-estimation of molecular volume but the error was much smaller. Finally, overall molecular dimensions increase with the carbon–proton interatomic distance, r_{C-H} ($\sim +10\%$ for $\Delta r_{C-H} = +0.03$ Å).

Table 3
100.6 MHz proton-coupled inversion-recovery data [a] for the lines of the carbon methine and methylene multiplets and one-bond heteronuclear coupling constants of UDP-Glc in the presence of monovalent cations (standard conditions)

Carbon	$^1J_{C,H}$ (Hz)	Apparent T_1 (ms)
C-1″	174	409, 496, 365, 415
C-4″	145	570, 449
C-6″	144	476, 251, 426
C-1′	168	422, 403
C-2′	150	621, 422
C-2′	151	622, 408
C-5′	150	378, 272, 321
C-5	177	479, 385
C-6	185	628, 392

[a] Data fitted for monoexponentiel recovery with the Bruker T_1 routine. Values correspond to lines from low (left) to high (right) field.

Cation complexation sites.—Interpretation of the NMR data ($\Delta\delta$ and T_1 values) recorded for UDP-Glc in the presence of metal cations requires a precise picture of the UDP-Glc–cation interactions: the fraction of molecules in the bound state, the number of binding sites, the atoms involved in the interaction, and the geometry of the complex. Strong interactions are observed for nucleoside di- and triphosphate–metal complexes ($UDP-Mg^{2+}$, $\log K \sim 3$ [15]) and it has been demonstrated that the preferred metal ion binding sites for uridine nucleoside di- and triphosphate–metal complexes are the phosphate oxygens [16,53].

In the case of carbohydrate–metal complexes [54–56], only certain sugar configurations (presenting adjacent axial–equatorial–axial and triaxial hydroxyl groups) lead to significant binding and for glucose very weak non-specific interactions through pairs of hydroxyl groups would be predicted.

Comparison of the ^{1}H and ^{13}C NMR chemical shift data for samples of UDP-Glc that have been acquired in the presence of monovalent cations (Na^{+}, K^{+}) with those of alkaline earth cations (Ca^{2+}, Mg^{2+}) in Tables 1 and 2 reveals only very small ($\Delta\delta < 0.05$ ppm) variations in the chemical shifts of UDP-Glc. In the case of sialic acid which forms a strong complex with Ca^{2+} (K_{assoc} 121 M^{-1}), the calcium-induced diamagnetic shifts for the protons and carbons closest to the cation were 0.316 (H-7) and 1.42 (C-8) ppm, respectively [57]. It can be concluded that in the presence of alkaline earth cations significant interaction with the UDP-Glc sugar moieties does not occur.

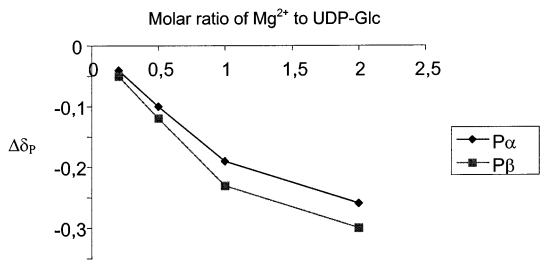

Fig. 5. Plots of the variations in the phosphorous chemical shifts as a function of the molar ratio of Mg^{2+} ions.

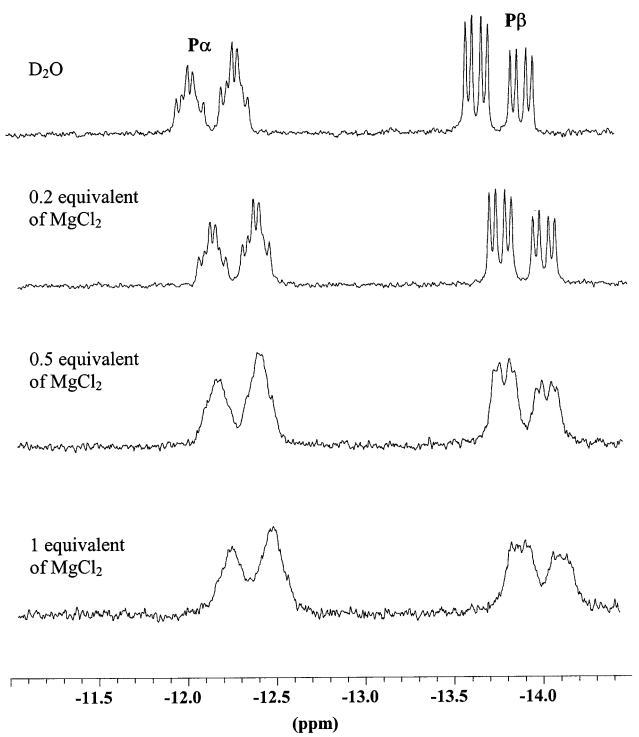

Fig. 6. 81 MHz ^{31}P spectra of UDP-Glc recorded under standard conditions (10 mM phosphate buffer in D_2O, 0.3 equiv of K^{+}, 2.7 equiv of Na^{+}) and in the presence of various molar ratios of Mg^{2+}.

In contrast, substantial diamagnetic shifts ($\Delta\delta$ values) were detected for the phosphate buffer signal, P_{α} (0.25 ppm), and P_{β} (0.30 ppm) in the presence of 2 equivalents of Mg^{2+}. The ^{31}P $\Delta\delta$ values have been plotted as a function of the ratio of Mg^{2+} to UDP-Glc in Fig. 5 and it can be seen that the diamagnetic shifts increase strongly up to a mole ratio of 1:1 and more slowly for higher ratios suggesting the formation of a strong 1:1 complex followed by possible weaker binding of additional Mg^{2+} ions. Comparison of the $\Delta\delta$ values of the UDP-Glc–Mg^{2+} complex with those reported in a study [58] of the Mg^{2+} chelation of triply-charged geranyl diphosphate (90% of association; 0.68 and 1.58 ppm, respectively, for the phosphorus α to the terpene, P_{α}, and the doubly charged P_{β}) indicates smaller effects for the former UDP-Glc–Mg^{2+} complex. The diamagnetic shifts of the phosphorus signals in Table 1 for the sample containing an equivalent of Ca^{2+} are much smaller than for those containing Mg^{2+} in agreement with the weaker chelation of di- and triphosphates by the former cation reported in the literature [15].

Close inspection of the 81 MHz ^{31}P spectra of UDP-Glc as a function of the UDP-Glc–Mg^{2+} ratio (Fig. 6) shows that both the P_{α}, and P_{β} signals broaden with increasing amounts of Mg^{2+}. Moreover, in the presence of UDP-Glc a strong increase in the ^{25}Mg linewidth is observed when compared to that of an aqueous solution of $MgCl_2$ (Fig. 7). In the case of ^{23}Na complexes of crown ethers [59] similar phenomena are usually interpreted in terms of fast quadrupole relaxation due to the lack of cubic symmetry around the quadrupolar ion in the complexed species when compared to the solvated species. In a

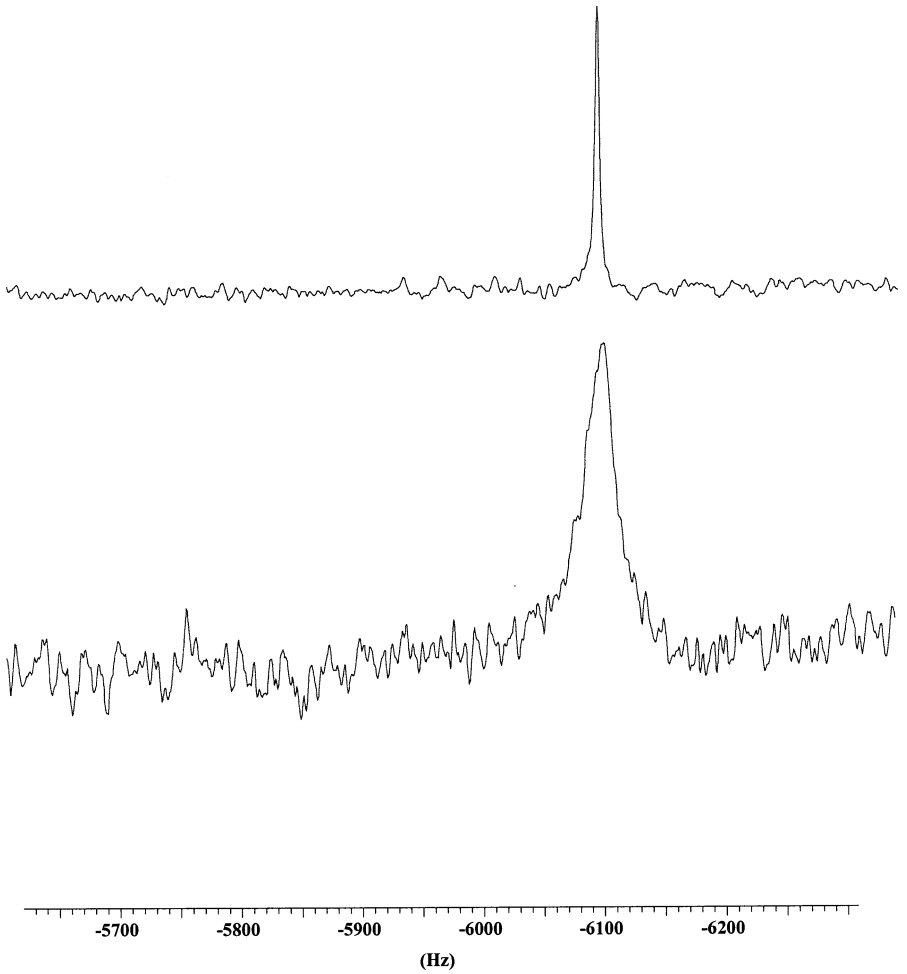

Fig. 7. 24.5 MHz ^{25}Mg NMR spectra of an aqueous solution of $MgCl_2$ (above, $\Delta\nu_{1/2}$ 4 Hz) and a 33 mM sample of UDP-Glc in the presence of 1 equiv of Mg^{2+} (below, $\Delta\nu_{1/2}$ 27 Hz).

series of ^{25}Mg spectra in which the $[Mg^{2+}]$/[UDP-Glc] ratio was varied systematically, the ^{25}Mg linewidths were fairly broad and constant for ratios of less than 1, then decreased rapidly until the ratio was close to 10 and finally narrowed much more slowly to attain a six-fold decrease for a $[Mg^{2+}]$/[UDP-Glc] ratio of 80 (fully complexed species). The low signal-to-noise ratio of the spectra recorded for low Mg^{2+} concentrations made it difficult to accurately estimate the linewidth of the fully-complexed species limiting the precision of the stability constant determined with this approach [60] but it can be surmised that the major species (90%) is the Mg^{2+}–UDP-Glc complex. Furthermore, line-narrowing was not observed for spectra recorded in a temperature range 25–80 °C indicating that the coalescence of free and complexed species occurred at much lower temperature and that chemical exchange was not contributing significantly to the linewidths. In the course of this study, slow transformation of UDP-Glc into uridine 5′-phosphate and α-D-glucopyranosyl 1,2-cyclic phosphate (characterized from ^{1}H, ^{13}C [9] and ^{31}P [61] chemical shift and coupling constant data) was observed for the samples containing the alkali-earth cations (Mg^{2+}, Ca^{2+}).

Selective line-broadening experiments (^{1}H, ^{13}C, ^{31}P, etc.) have often been used to reveal the formation of complexes between paramagnetic species and organic molecules [62,63]. The ^{1}H longitudinal relaxation times for solutions of UDP-Glc containing 0.003 equiva-

lents of Mn^{2+} and 1 equivalent of Mg^{2+} have been collected in Table 4. The reduction in proton T_1 values in the presence of Mn^{2+} is striking. The shortest proton T_1 is observed for H-1″ (32 ms) followed by H-5′b (45 ms) and H-6 (93 ms) indicating that these protons are the closest to the paramagnetic species. These data would be compatible with a complex in which the Mn^{2+} ion was located roughly between the two phosphate moieties. Similar conclusions can be drawn from the plots of the methine carbon longitudinal relaxation rates as a function of the Mn^{2+} concentration in Fig. 8. The largest slope is detected for the glucose anomeric carbon followed by ribosyl C-3′ and C-4′ indicating that these spins have the closest contacts with the paramagnetic species. ^{31}P spectra were also recorded for these samples and severe line-broadening is observed for the phosphate buffer, the P_α, and the P_β resonances in agreement with complexation of Mn^{2+} by both P_α, and P_β phosphate oxygens.

Table 4
400 MHz ^1H longitudinal relaxation times, T_1 (in ms), of a 33 mM solution of UDP-Glc in the presence of divalent cations (0.003 equiv Mn^{2+} and 1 equiv Mg^{2+}) at 298 K

Protons	Mn^{2+} T_1 (ms)	Mg^{2+} T_1 (ms)
H-1″	32	1355
H-2″	183	1291
H-3″	130	824
H-4″	328	1236
H-5″	97	699
H-6″a	125	635
H-6″b	139	507
H-1′	205	2503
H-2′, H-3′	132 [a]	1121
H-4′	132	685
H-5′a	132	475
H-5′b	45	398
H-5	205	2481
H-6	93	1081

[a] Overlapping resonances.

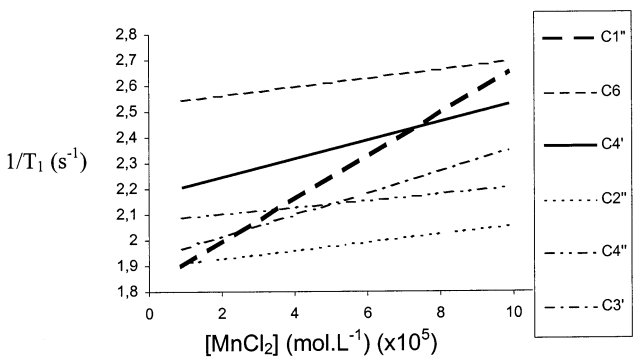

Fig. 8. Plots of the 100.6 MHz carbon relaxation rates of the methine carbons of UDP-Glc as a function of the molar ratio of Mn^{2+}.

Molecular dimensions and intersugar distances of model structures.—The v_1 and v_2 torsion angles of the pyrophosphate moiety of the disodium salt of UDP-Glc adopt a staggered conformation in the crystal [11] whereas an eclipsed geometry is required to obtain the 2.8 Å distance between the phosphate oxygens displayed in crystal structures where the pyrophosphate group acts as a bidentate ligand. As described in Section 2, molecular models of UDP-Glc corresponding to staggered (0, 180°) and eclipsed (134, 102°) arrangements of the pyrophosphate moiety with the two sugar residues positioned in the trans orientation (Fig. 2(b)) were used to summarily explore the conformational space of the pyrophosphate group (Ψ and α torsion angles in 60° steps) affording two sets of 36 structures. The other torsion angles (sugar puckering, Φ, β, γ and χ) were set to the NMR-defined values and no attempt was made to optimize these structures as realistic molecular modeling of medium-sized charged molecules such as UDP-Glc with appropriate methods such as molecular dynamics simulations requires both the presence of counterions and explicit solvent. The length of UDP-Glc (maximum extension, L) and the two NOE-defined distances between the sugar moieties ($d_{1''-5'proR}$, and $d_{1''-5'proS}$ distances) were monitored for these sets of conformers to obtain a rough picture of plausible ranges for these parameters. The average values for these distances for the two sets of structures are collected in Table 5.

It can be seen that the average length of the UDP-Glc molecule is similar for both eclipsed (14.4 Å, 36 structures) and staggered (13.8 Å, 36 structures) arrangements of the pyrophosphate groups and the average interglycosyl distances are much too long (>5.4 Å) to generate the weak experimental NOE values detected between H-1″ and H-5′proR or H-5′proS. As none of these geometries presented

Table 5
Average distance data [a] for sets of uridine diphosphoglucose structures with the pyrophosphate moiety in either the trans-eclipsed or trans-staggered (v_1 0°, v_2 180°) arrangements. Conformers were obtained by varying the Ψ and α dihedrals in 60°-steps while maintaining the NMR-defined values of the other torsion angles (sugar puckering [b], Φ, ω, β, γ, and χ)

	L (Å)	trans-Eclipsed (v_1 134°, v_2 102°)		L (Å)	trans-Staggered (v_1 0°, v_2 180°)	
		$d_{1'',5'\text{proR}}$ (Å)	$d_{1'',5'\text{proS}}$ (Å)		$d_{1'',5'\text{proR}}$ (Å)	$d_{1'',5'\text{proS}}$ (Å)
Total set (36 structures)	14.4	6.0	5.9	13.8	5.6	5.4
NMR-compatible	15.0 [c]	4.8 [c]	4.7 [c]	13.6 [d]	4.8 [d]	4.7 [d]

[a] The L values correspond to the average value of largest interatomic distance for the specified set of structures.
[b] The values in the table correspond to C-2′-endo puckering but similar data were estimated for the C-3′-endo conformer.
[c] This set includes: $0 < \Psi < 120$, all values of α except the 150–270° range.
[d] This set includes: $-60 < \Psi < 60$, all values of α.

short contacts (< 3 Å) that alone would be capable of generating the experimental NOE values if they represented a significant fraction (5–10%) of the time-averaged population, it appears that most of the UDP-Glc structures that constitute the conformational mixture in solution must display borderline (~ 5 Å) intersugar distances. When the average L was computed considering only the structures in each set with such $d_{1'',5'\text{proR}}$ and $d_{1'',5'\text{proS}}$ values ($3.5 < r_{H,H} < 5.0$ Å), a significant increase in the average length of the structures with the pyrophosphate group in the eclipsed arrangement (15.0 Å) as compared to the staggered form (13.6 Å) was observed. These results would explain the more extended conformation of UDP-Glc in the presence of Mg^{2+} as compared to monovalent cations (Na^+, K^+) that has been estimated from ^{13}C longitudinal relaxation times and hydrodynamic theory.

4. Conclusions

The present study has shown that in the presence of monovalent cations UDP-Glc adopts a fairly extended average overall shape. Analysis of the proton, carbon, and phosphorous diamagnetic shifts for samples containing divalent cations has shown that the phosphate oxygens are the preferred coordination sites. Magnesium ions form a stronger complex (roughly 90% in the bound state from ^{25}Mg NMR) than calcium ions and the UDP-Glc–Mn^{2+} complex displays similar features with coordination occurring at the phosphate oxygens. Carbon relaxation data have shown that magnesium ions lead to a significant increase in the average length of the UDP-Glc molecule as compared to monovalent cations. The NMR-defined average molecular shape is compatible with eclipsed arrangements of the pyrophosphate group necessary for bidentate chelation of the cation. These results corroborate the hypothesis that the role of the metal ion in enzymic reactions involving nucleotide sugars may be to preorganize the nucleotide sugar. It can be seen from the schematic models in Fig. 2(b) (which were originally proposed for pyrophosphates) that, in the case of nucleotide sugars, metal ion chelation not only temporarily positions the glucosyl and ribosyl sugars either cis or trans with respect to the newly-created six-membered ring but also introduces two additional assymmetric centers at the phosphorous atoms.

In future work, the experimental data described in this account will be used to validate MD simulations of UDP-Glc in the presence of explicit water and mono- and divalent cations.

Acknowledgements

One of us (C.M.) acknowledges support from the French Ministère de l'Enseignement Supérieur et de la Recherche. The authors also thank Dr A. Imberty and P. Petrova for stimulating discussions.

References

[1] N.K. Kochetkov, V.N. Shibaev, *Adv. Carbohydr. Chem. Biochem.*, 28 (1973) 307–397.
[2] M.M. Palcic, O. Hindsgaul, *Trends Glycosci. Glycotechnol.*, 8 (1996) 37–49.
[3] S. David, *Chimie moléculaire et supramoléculaire des sucres*, CNRS, Paris, 1995, pp. 169–176.
[4] C.E. Cardini, A.C. Paladini, R. Caputto, L.F. Leloir, *Nature*, 165 (1950) 191–192.
[5] E. Cabib, L.F. Leloir, C.E. Cardini, *J. Biol. Chem.*, 203 (1953) 1055–1070.
[6] E.I. Budowsky, T.N. Drushinina, G.I. Eliseeva, N.D. Gabrielyan, N.K. Kochetkov, M.A. Novikova, V.N. Shibaev, G.L. Zhdanov, *Biochim. Biophys. Acta*, 122 (1966) 213–224.
[7] S. Hirano, *Biochem. Biophys. Res. Commun.*, 43 (1971) 1219–1222.
[8] C.H. Lee, R.H. Sarma, *Biochemistry*, 15 (1976) 697–704.
[9] J.V. O'Connor, H.A. Nunez, R. Barker, *Biochemistry*, 18 (1979) 500–507.
[10] R.E. London, A.D. Sherry, *Biochemistry*, 17 (1978) 3662–3666.
[11] Y. Sugawara, H. Iwasaki, *Acta Crystallogr., Sect. C*, 40 (1984) 389–393.
[12] A. Vrielink, W. Rüger, H.P.C. Driessen, P.S. Freemont, *EMBO J.*, 13 (1994) 3413–3422.
[13] L.N. Gastinel, C. Cambillau, Y. Bourne, *EMBO J.*, 18 (1999) 3546–3557.
[14] S.J. Charnock, G.J. Davies, *Biochemistry*, 38 (1999) 6380–6385.
[15] A.T. Tu, M.J. Heller, in H. Sigel (Ed.), *Metal Ions in Biological Systems: Simple Complexes*, Vol. 1, Marcel-Dekker, New York, 1974, pp. 1–116.
[16] W. Saenger, *Principles of Nucleic Acid Structure*, Springer, New York, 1984, pp. 201–219.
[17] J.J. Pavelites, J. Gao, P.A. Bash, A.D. Mackerell, *J. Comput. Chem.*, 18 (1997) 221–239.
[18] I. Tvaroska, I. Andre, J.P. Carver, *J. Phys. Chem.*, 103 (1999) 2560–2569.
[19] P. Petrova, J. Koca, A. Imberty, *J. Am. Chem. Soc.*, 121 (1999) 5535–5547.
[20] K.B. Kim, E.C. Behrman, E.J. Behrman, *Nucleotides Nucleosides*, 18 (1999) 1055–1056.
[21] D.E. Woessner, *J. Chem. Phys.*, 37 (1962) 647–654.
[22] F. Heatley, *Annu. Rep. NMR. Spectrosc.*, 17 (1986) 179–230.
[23] G. Lipari, A. Szabo, *J. Am. Chem. Soc.*, 104 (1982) 4546–4559.
[24] R.H. Marchessault, S. Pérez, *Biopolymers*, 18 (1979) 2369–2374.
[25] IUPAC–IUB, *Arch. Biochem. Biophys.*, 145 (1971) 405.
[26] D. Marion, K. Wüthrich, *Biochem. Biophys. Res. Commun.*, 113 (1983) 967–974.
[27] D.J. States, R.A. Haberkorn, D.J. Ruben, *J. Magn. Reson.*, 48 (1982) 286–292.
[28] U. Piantini, O.W. Sorensen, G. Bodenhausen, G. Wagner, R.R. Ernst, K. Wüthrich, *J. Am. Chem. Soc.*, 104 (1982) 6800–6802.
[29] C. Griesinger, G. Otting, K. Wüthrich, R.R. Ernst, *J. Am. Chem. Soc.*, 110 (1988) 7870–7873.
[30] M.F. Summers, L.G. Marzilli, A. Bax, *J. Am. Chem. Soc.*, 108 (1986) 4285–4294.
[31] D.C. McCain, J.L. Markley, *J. Am. Chem. Soc.*, 108 (1986) 4259–4264.
[32] B. Brooks, R. Bruccoleri, B. Olafson, D. States, S. Swaminathan, M. Karplus, *J. Comput. Chem.*, 4 (1983) 187–217.
[33] A.D. Buckingham, *Can. J. Chem.*, 38 (1960) 300–307.
[34] J.G. Batchelor, *J. Am. Chem. Soc.*, 97 (1975) 3410–3415.
[35] I. Solomon, *Phys. Rev.*, 99 (1955) 559–565.
[36] N. Bloembergen, *J. Chem. Phys.*, (1957) 572–573.
[37] M.M. Tirado, J.G. de la Torre, *J. Chem. Phys.*, 73 (1979) 1986–1993.
[38] J.G. de la Torre, V.A. Bloomfield, *Q. Rev. Biophys.*, 14 (1981) 81–139.
[39] K. Bock, J.O. Duus, *J. Carbohydr. Chem.*, 13 (1994) 513–543.
[40] C.A.G. Haasnoot, F.A.A.M. de Leeuw, C. Altona, *Tetrahedron*, 36 (1980) 2783–2792.
[41] F.E. Hrusha, D.J. Wood, R.J. Mynott, R.H. Sarma, *FEBS Lett.*, 31 (1973) 153–155.
[42] D.J. Wood, F.E. Hrusha, R.J. Mynott, R.H. Sarma, *Can. J. Chem.*, 51 (1973) 2571–2577.
[43] M.M.W. Mooren, S.S. Wijmenga, G.A. van der Marel, J.H. van Boom, C.W. Hilbers, *Nucleic Acids Res.*, 22 (1994) 2658–2666.
[44] P. Dais, *Adv. Carbohydr. Chem. Biochem.*, 51 (1995) 63–131.
[45] N. Bouchemal-Chibani, C. Hervé du Penhoat, M. Ghomi, A. Laigle, C. Derouet, P.Y. Turpin, *Biopolymers*, 39 (1996) 549–571.
[46] N. Bouchemal-Chibani, I. Braccini, C. Hervé du Penhoat, V. Michon, *Int. J. Biol. Macromol.*, 17 (1995) 177–182.
[47] V.A. Daragan, K.H. Mayo, *Progr. NMR Spectrosc.*, 31 (1997) 63–105.
[48] R.T. Boeré, R.G. Kidd, *Annu. Rep. NMR Spectrosc.*, 13 (1982) 319–385.
[49] M. Hricovini, G. Torri, *Carbohydr. Res.*, 268 (1995) 159–175.
[50] L.E. Kay, L.K. Nicholson, F. Delaglio, A. Bax, D.A. Torchia, *J. Magn. Reson.*, 97 (1992) 359–375.
[51] A.G. Palmer, N.J. Skelton, W.J. Chazin, P.E. Wright, M. Rance, *Mol. Phys.*, 75 (1992) 699–711.
[52] A.D. Bain, R.M. Lynden-Bell, *Mol. Phys.*, 30 (1975) 325–356.
[53] E. Walaas, *Acta Chem. Scand.*, 12 (1958) 528–536.
[54] S.J. Angyal, *Adv. Carbohydr. Chem. Biochem.*, 47 (1989) 1–43.
[55] K. Dill, R.D. Carter, *Adv. Carbohydr. Chem. Biochem.*, 47 (1989) 125–166.
[56] D.M. Whitfield, S. Stojkovski, B. Sarkar, *Coord. Chem. Rev.*, 122 (1993) 171–225.
[57] L.W. Jaques, E.B. Brown, J.M. Barrett, W.S. Brey, W Weltner, *J. Biol. Chem.*, 252 (1977) 4533–4538.
[58] D.I. Ito, S. Izumi, T. Hirata, T. Suga, *J. Chem. Soc., Perkin Trans. I*, (1992) 37–39.
[59] G.W. Buchanan, *Progr. NMR Spectrosc.*, 34 (1999) 327–377.
[60] M.-D. Tsai, T. Drakenberg, E. Thulin, S. Forsén, *Biochemistry*, 26 (1987) 3635–3643.
[61] R. Fathi, F. Jordan, *J. Org. Chem.*, 51 (1986) 4143–4146.
[62] K. Dill, R.D. Carter, *Adv. Carbohydr. Chem. Biochem.*, 47 (1989) 125–166.
[63] G.C. Levy, J.J. Dechter, *J. Am Chem Soc.*, 102 (1980) 6191–6196.